communications biology

Article

https://doi.org/10.1038/s42003-024-06750-0

Structural shifts in TolC facilitate Efflux-Mediated β-lactam resistance

Check for updates

Isik Kantarcioglu [1,2], Ilona K. Gaszek [2], Tandac F. Guclu [1], M. Sadik Yildiz[2], Ali Rana Atilgan [1], Erdal Toprak [2,3] ✉ & Canan Atilgan [1,3] ✉

Efflux-mediated β-lactam resistance is a major public health concern, reducing the effectiveness of β-lactam antibiotics against many bacteria. Structural analyses show the efflux protein TolC in Gram-negative bacteria acts as a channel for antibiotics, impacting bacterial susceptibility and virulence. This study examines β-lactam drug efflux mediated by TolC using experimental and computational methods. Molecular dynamics simulations of drug-free TolC reveal essential movements and key residues involved in TolC opening. A whole-gene-saturation mutagenesis assay, mutating each TolC residue and measuring fitness effects under β-lactam selection, is performed. Here we show the TolC-mediated efflux of three antibiotics: oxacillin, piperacillin, and carbenicillin. Steered molecular dynamics simulations identify general and drug-specific efflux mechanisms, revealing key positions at TolC's periplasmic entry affecting efflux motions. Our findings provide insights into TolC's structural dynamics, aiding the design of new antibiotics to overcome bacterial efflux mechanisms.

TolC is an outer membrane protein with a critical role in antibiotic efflux

Gram-negative bacteria have evolved transport mechanisms to move macromolecules and toxic compounds across membranes[1]. These mechanisms play important roles in drug resistance to current and future antibiotics[2]. Bacterial efflux is one of the primary systems responsible for the emergence of multidrug resistance since efflux machineries in bacteria can pump out several different types of antibiotics with varying rates and specificity[3,4]. The resistance-nodulation-division (RND) family is one of the major efflux pump superfamilies in Gram-negative bacteria that can efflux a broad range of substrates, including clinically important antibiotics such as β-lactams, bile salts, and detergents[5,6]. The major multidrug-resistant efflux pump in *Escherichia coli* (*E. coli*) is the AcrAB-TolC protein complex[7]. In *E. coli*, the outer membrane protein TolC can transiently associate with the protein pairs AcrAB, MacAB, and EmrAB to create various tripartite efflux pump assemblies as a response to elevated antibiotic concentrations inside bacteria[8]. These efflux assemblies, which span the length of the periplasmic space, expel toxic substances from the cytoplasm to the extracellular region. Understanding specificity of the efflux pumps towards various substrates will lead to drug development strategies to avoid or inhibit them[9].

TolC is a multifunctional protein that is subject to conflicting evolutionary selection pressures. While TolC is crucial to protect bacterial cells against antibiotics and other antibacterial compounds, its presence can impose a risk for bacterial cells, since TolC can also function as a portal for the transport of bacteriocins and bacteriophages into the cells (Fig. 1A)[10]. Thus, bacteria need to strike an evolutionary balance between making TolC available when efflux is necessary and limiting it as an entry point when efflux presents risk[11].

Structural studies reveal that TolC functions as a homotrimer. Its 12-stranded β-barrel part is embedded into the outer membrane and is approximately 40 Å long; its cone-like α–helical coiled-coil domain extends into the periplasm (Fig. 1B) spanning an additional 100 Å[12]. The outer membrane channel opening, especially periplasmic end opening, is necessary to initiate the process of the expulsion of the antibiotic molecules[13]. We note that TolC's role in antibiotic efflux is highly dependent on its interactions in the resulting AcrAB-TolC complex. The conformational state of AcrB has been proposed to be transmitted to TolC by AcrA, leading to the opening of TolC[14]. Mutations in the periplasmic tip of TolC have been shown to change this communication within the AcrAB-TolC complex[13,15,16]. Bavro et al. investigated the importance of a network of hydrogen bonds and salt bridges involving Y362 and R367 to maintain the closed state of TolC. Y362F/R367E double mutants disrupted this network which resulted in increased sensitivity to vancomycin[13]. Pei et al. proposed the importance of T152, D153, Y362, and R367 to constrain the molecule efflux. R367S mutation increased the channel's conductance up to 4-fold and the Y362F/R367S double mutation by nearly 15-fold. It has been proposed that the destabilization of ionic and hydrogen bonds at the periplasmic tip could dilate the TolC pore entrance and allow substrate

[1]Faculty of Engineering and Natural Sciences, Sabancı University, Tuzla, Istanbul, Turkey. [2]Department of Pharmacology, University of Texas Southwestern Medical Center, Dallas, TX, USA. [3]These authors contributed equally: Erdal Toprak, Canan Atilgan. ✉e-mail: erdal.toprak@utsouthwestern.edu; canan@sabanciuniv.edu

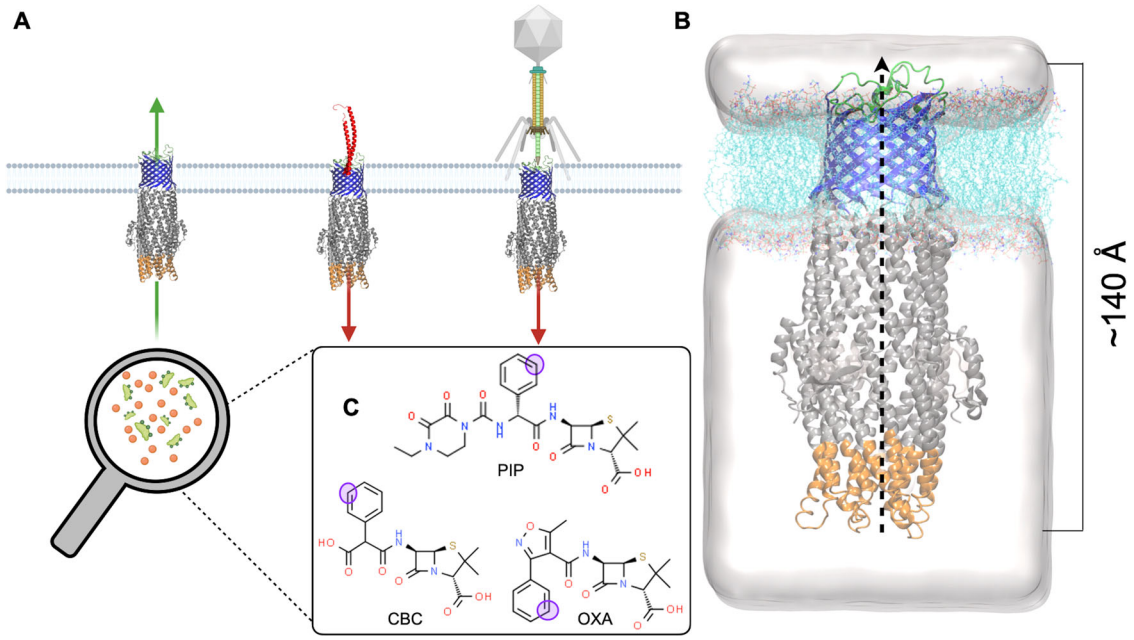

Fig. 1 | TolC and ligand structures. A TolC structure positioned in outer membrane. The major known role of TolC in *E. coli* is to expel antibiotics and bile salts to the outside of the cell which is essential for bacterial survival (green arrow). However, it is also an entry point for colicin-E1 (partial structure shown in red) and some bacteriophages which results in cell death (red arrow) (Created with BioRender.com). **B** TolC embedded in a POPE lipid membrane (cyan) and placed in a simulation box shown as a white blob; extracellular loops are colored in green, membrane embedded β-barrel is colored in blue, a-helices extended through periplasmic space are colored in gray and the approximately 30 Å part located at the periplasmic tips of the protein is colored in orange. This coloring scheme is maintained throughout the manuscript. The reaction coordinate of the drug is defined from the entry point to the exit and spans ~140 Å (dashed line). **C** Two-dimensional representations of the antibiotics studied in this work. Carbenicillin (CBC), piperacillin (PIP), and oxacillin (OXA); SMD pulling atoms for the drug molecules are shown as purple circles.

passage[15]. D371V is another highlighted mutation which has notable impact on growth even without the presence of antibiotics, leading to increased susceptibility to tested substrates. The study identified antibiotic-specific phenotypes linked to mutations in TolC, indicating that substrate specificity may not be exclusively determined by the transporter protein or the periplasmic adaptor protein (PAP). Instead, it suggests that the TolC channel itself may also play a significant role in determining substrate specificity[16]. Nevertheless, the role of TolC-drug interactions on the rate of efflux and TolC's contributions to the selectivity once the drug has been delivered to its channel have not been interrogated.

Previous biophysical studies utilizing computational tools uncovered important structural regions and rearrangements in TolC and its homologs

Outer membrane protein OprM from *Pseudomonas aeruginosa* is one of the closest homologs of *E. coli* TolC. Normal mode analysis (NMA) based on elastic network models[17] was previously used to uncover the conformational states of OprM and how they compare to the open state of TolC[18]. In the closed form of TolC, coiled-coil helices linked by salt bridges and hydrogen bonds at the tip of the periplasmic entrance provide selectivity and constrictions for substance transport, particularly maintained by D371 and D374[13,15]. CmeC found in *Campylobacter jejuni* is another homologue that shares structural similarities with TolC. Substrate efflux mechanisms with CmeC have also been simulated by others[19] using steered molecular dynamics (SMD) simulations[20]. Their results indicated the anionic bile acid moves up the channel by climbing a ladder of acidic residues that align in the interior surface of the protein. Unlike CmeC, TolC has far fewer charged residues along the efflux path, which indicates a different action mechanism.

These findings and the critical importance of TolC in antibiotic resistance motivate our exploration of the structural shifts in the TolC protein at the atomistic level. We first utilized molecular dynamics (MD) simulations for both the closed and the open forms of drug-free TolC to determine its intrinsic dynamics and structural transitions that are difficult to observe by most experimental methods. Principal component analysis[21,22] of MD trajectories suggested that TolC has an intrinsic expelling movement in both closed and open forms. The dominant modes of these forms displayed net movement in the direction of efflux and, hence, suggest these modes may play an important role in expelling antibiotic molecules. Since TolC conformations can switch between closed and open forms, we hypothesized that there must be important residues whose perturbation might tip the equilibrium between the two conformations.

To systematically search for these residues, we utilized the perturbation response scanning (PRS) that we previously developed as a robust and now a widely used method for identifying essential residues that trigger conformational changes of proteins[23,24]. PRS relies on linear response theory to determine specific residues that, when perturbed via external forces, might lead to conformational changes in proteins; PRS has been successfully used by several groups to identify structurally important regions not only in many monomeric proteins but also in multimeric assemblies such as HSP90[25]. PRS also was applied to unravel motions that trigger uncoating when applied to a multiprotein capsid comprised of 60 protomeric units, each of which contained four heterogenic subunits[26].

We explored dynamical shifts within the TolC structure that enable the efflux of three β-lactam antibiotics: carbenicillin, piperacillin, and oxacillin, as illustrated in Fig. 1C

The choice of β-lactam antibiotics was due to their great importance in fighting against bacterial infections and the rapid evolution of β-lactam resistance in clinical and community settings. Almost 80 percent of all antibiotics used in clinics are β-lactams. Although resistance to β-lactams is often attributed to spread of β-lactamase genes producing β-lactamases that render β-lactams ineffective by hydrolyzing them, many β-lactam antibiotics are ineffective against Gram-negative bacteria because of their fast efflux from the cytoplasm. For instance, we previously showed that disruption of the AcrAB-TolC complex in *E. coli* can reduce the required dose of oxacillin to kill bacterial cells by almost three orders of magnitude[10]. We

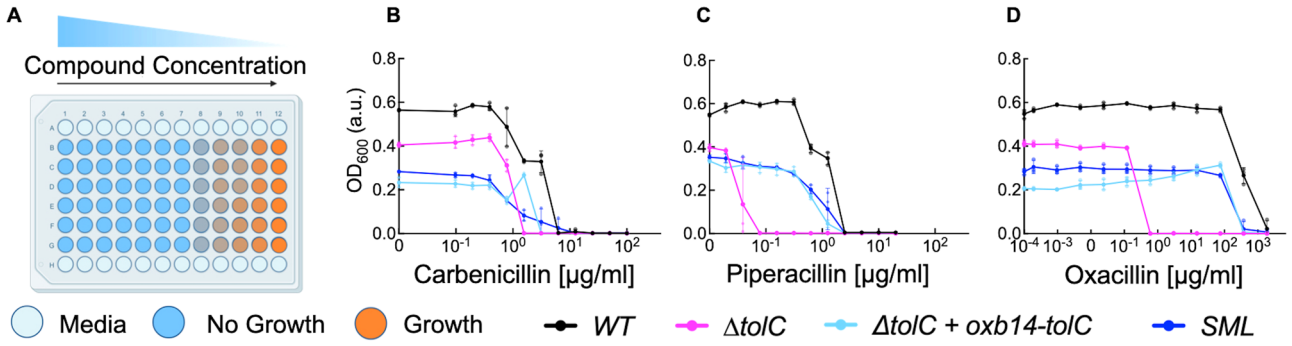

Fig. 2 | Minimum inhibitory concentration (MIC) measurements. A MIC assay plate setup. Blue wells indicate no growth; color gradation towards orange indicates the level of growth (Created with BioRender.com). **B**–**D** Three different antibiotics were used as selection factors. We incubated three strains and the Single Mutation Library (SML, Methods) in the presence of increasing drug concentrations and monitored bacterial growth for ~18 h. Black line represents dose response curves for wild type (BW25113) *E. coli* strain. Magenta lines represent *E. coli* strain with *tolC* gene deletion (*ΔtolC*). Cyan lines represent *ΔtolC*+pOxb14*tolC*. Blue lines represent SML strain which contains all possible amino acid mutations. Background-corrected OD600 values after 18 hours of incubation measure cell growth on the y-axis, with error bars showing standard deviations across three replicates per concentration, $N = 3$. Lines connect the means of sample size $N = 3$ for each drug at each concentration; dots represent individual data points. Raw data with background corrections is provided in Supplementary Table S1.

chose oxacillin, piperacillin, and carbenicillin for our study due to the distinct efflux efficiencies of the AcrAB-TolC complex towards these antibiotics—high for oxacillin, moderate for piperacillin, and low for carbenicillin. To substantiate these efficiencies, we compared the minimum inhibitory concentrations (MICs) needed to inhibit a wild-type *E. coli* strain, a *tolC*-deficient mutant, and the mutant harboring a *tolC*-carrying rescue plasmid, as shown in Fig. 2.

We also systematically explored the fitness effects of single amino acid replacements at each position in TolC using a saturation mutagenesis library under selection with each of these drugs. Finally, we utilized SMD simulations to calculate work curves during passage of these drug molecules through TolC homotrimer opening to determine drug specific and generalist TolC residues involved in β-lactam efflux.

Results and Discussion

TolC dynamics are inherently optimized for efflux

We performed MD simulations to gain insights about TolC structural dynamics for closed and open states of the wild type TolC (Fig. 3A). Root-mean square fluctuations of the residues (RMSFs) were highest at the periplasmic side for all simulated structures (Fig. 3B). However, the fluctuations were greater on the periplasmic side in the open form, and on the outer membrane side in the closed form, which might be indicative of the changes in the closing/opening motion of the protein (Fig. 3B). Finally, the larger fluctuations near residue 200 correspond to the equatorial domain helices in the widest region of the protein contacting water and are not functionally relevant. Consequently, their mobility remains the same irrespective of the open/closed forms.

The greatest conformational changes were observed in the H7/H8 helices. H3/H4 helices were comparatively stable (Fig. 3C)[13,27,28]. D371 and D374 on H8 are at the points of the two of the narrowest constrictions[27]. In fact, D371 was shown to be important in gating, with increased susceptibility to various substances in the D371V mutant. R367 is another site that makes strong interactions to hold inter-protomer and intra-protomer helices together (R367-D153 and R367-T152 for the former and Y362-D153 for the latter)[16]. Since TolC is a homotrimer, we calculated the triangular cross-sectional area (TCA) using the C_α atoms of these specific residues, R367, D371, and D374, which form a ladderlike entry region into the pore used in efflux (Fig. 3D). TCAs for the open structure are expectedly much larger than the closed form. However, the largest area is at the level of the innermost D374 residue in the closed form while the reverse is true for the open form, i.e., the truncated cone formed by these three residues is reversed during opening (Fig. 3E).

To understand the underlying motions that collectively orchestrate TolC dynamics in the absence of drugs, we monitored the principal components (PCs) obtained from the trajectories. Our aim for doing these calculations was to check if the collective modes describe intrinsic motions with a clear directionality from the periplasmic to the extracellular side, so that even in the absence of AcrAB in our model, TolC would provide relevant information for efflux. The top three PCs have similar amounts of contributions to the dynamics in the closed form, while the most collective mode of motion is more separated than the rest in the open form (Fig. 4A). In its closed form, the primary motion (PC1) induces a torque along the efflux axis in the lower half and a stretching opening in the upper half; the reverse is true for PC2. PC3 is an upward pumping motion (see Supplementary Videos 1–3). In the open form, motions in the open periplasmic side overwhelm the dynamics, while PC2 and PC3 overlap with the top two PCs of the closed form (see Supplementary Videos 4–6). Thus, TolC remains primed for efflux even in the absence of drugs, more so when closed than open.

PRS calculations determined the key residues involved in triggering the open-to-closed and closed-to-open conformational changes (Fig. 4B, C).

Our findings show that the closed-to-open correlation coefficients, C_i, are significantly lower than open-to-closed ones, suggesting the protein naturally tends to close from an open state and requires specific residue perturbations for opening from a closed state. Despite the less stringent selection of the threshold we employed, we found far fewer residues that can enforce channel opening. Moreover, residues located on the H7/H8 helices have higher C_i values than the H3/H4 helices, reinforcing the active role of the former pair of helices in channel opening as previously reported[13,27]. Aligning with previous determinations, our results confirmed the closed form as TolC's stable state, upon which we based our continued simulations.

TolC facilitates drug efflux through dynamic changes in a critical interaction network

We used steered molecular dynamics (SMD) simulations to track the work produced as antibiotics move through TolC (Fig. 5A). We calculated the average work to transport from the periplasmic to the extracellular side, with the order being carbenicillin > piperacillin > oxacillin. We also monitored the drug-protein interactions along this path (Fig. 5B–D). We found common interactions for all antibiotic molecules we tested at the extracellular side during the final exit of the antibiotic (those in the green stripe region in Fig. 5). However, carbenicillin formed more bonds than the other antibiotics, correlating with our findings that its efflux rate through *E. coli* TolC is lower. The rise in hydrogen bonds during carbenicillin's transfer increased energy expenditure, prompting us to explore if this was due to direct contacts with TolC. Our analysis revealed that the average number of hydrogen bonds with TolC's pore lining and the derivative of average work shared similar patterns, albeit with a slight shift on the reaction coordinate

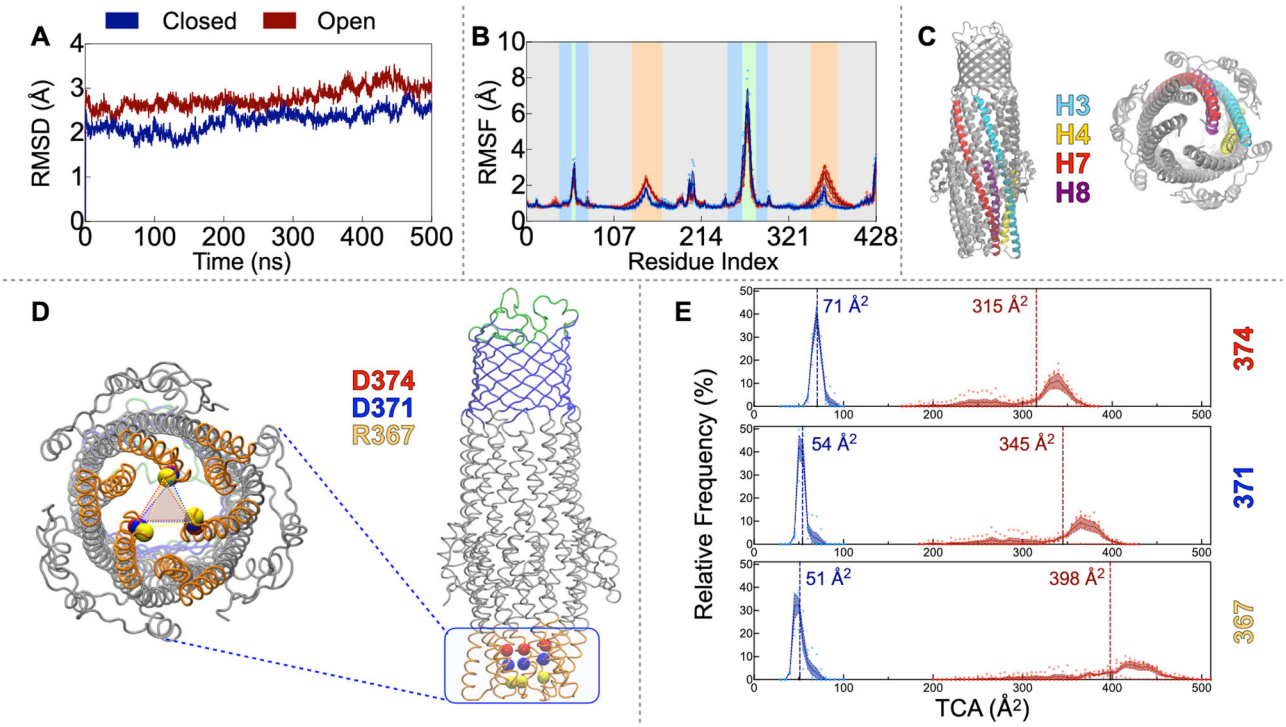

Fig. 3 | Molecular dynamics of ligand-free TolC. A C_α RMSDs of TolC remain in the 2–4 Å range during the 500 ns MD trajectories of both closed (blue), and open (red) forms ($N = 2500$ frames). **B** C_α RMSFs; colored vertical stripes follow the coloring of the TolC regions Fig. 1B: green extracellular loops, orange periplasmic entry region, blue β-barrel, gray the rest. Standard error of the mean (SEM) obtained from the average of the homotrimeric chains of the protein are shown as shades ($n = 3$ from the 428 residue-long monomers that compose TolC protein). **C** Specific four helices of one TolC protomer highlighted; side and bottom views; residue indices: H3 cyan (78–145), H4 yellow (151–185), H7 red (297–363), and H8 magenta (369–403). **D** Selected pore constricting trimeric C_α atoms visualized as spheres on the protein (R367 yellow, D371 blue, D374 red); the bottom view highlights the triangular shape. **E** Triangular cross-sectional area (TCA) histograms of residues in (**D**) ($N = 5$, 500 ns long closed and open form simulations were split into 5 equal chunks and the relative frequency distribution for TCA histograms were plotted. The bin size is 5. Individual relative frequency distribution data were represented with shades).

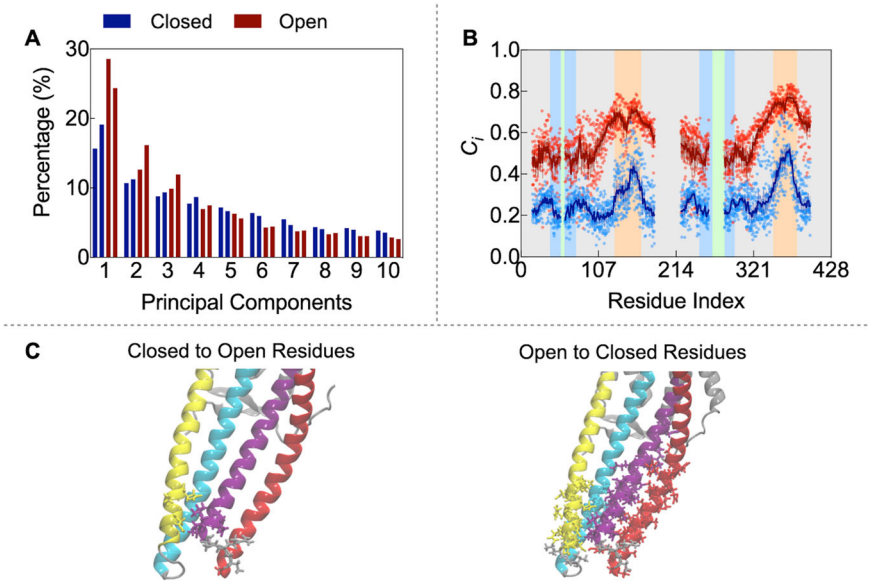

Fig. 4 | Collective motions of TolC. A Contribution of the top 10 PCs, obtained from two separate trajectory pieces (240–280 ns and 460–500 ns) in each of the closed (blue) and open (red) form simulations. **B** Pearson correlation coefficients obtained from PRS for closed and open forms. $N = 6$ obtained from two separate trajectory chunks from MD simulations and three identical monomers. Highest mobility regions excluded in the construction of the correlation matrix to capture motions of the main structure appear as disconnected regions in the graphs. 321 residues of 428 residue-long monomer were subjected to PRS calculations. Data represent mean ± SEM while scattered dots represent each Pearson correlation coefficient from PRS. SEM shown as shades (The *p*-values were calculated by one-sample two-tailed t-test. *P-values* of 63 residues from closed to open calculations and 13 residues from open to closed calculations were < 0.01, and the rest of them have *p*-values < 0.001). **C** PRS determines single residues implicated in channel opening mainly located on four helices shown in (**C**). Top-ranked residues for opening ($C_i > 0.50$): 160, 366-369, 369-374; top-ranked residues for closing ($C_i > 0.70$): 129,132,133,135–137,140,149,150,152–164,341-377. D371 has the highest correlation value of 0.54 and 0.82, respectively for closed and open forms.

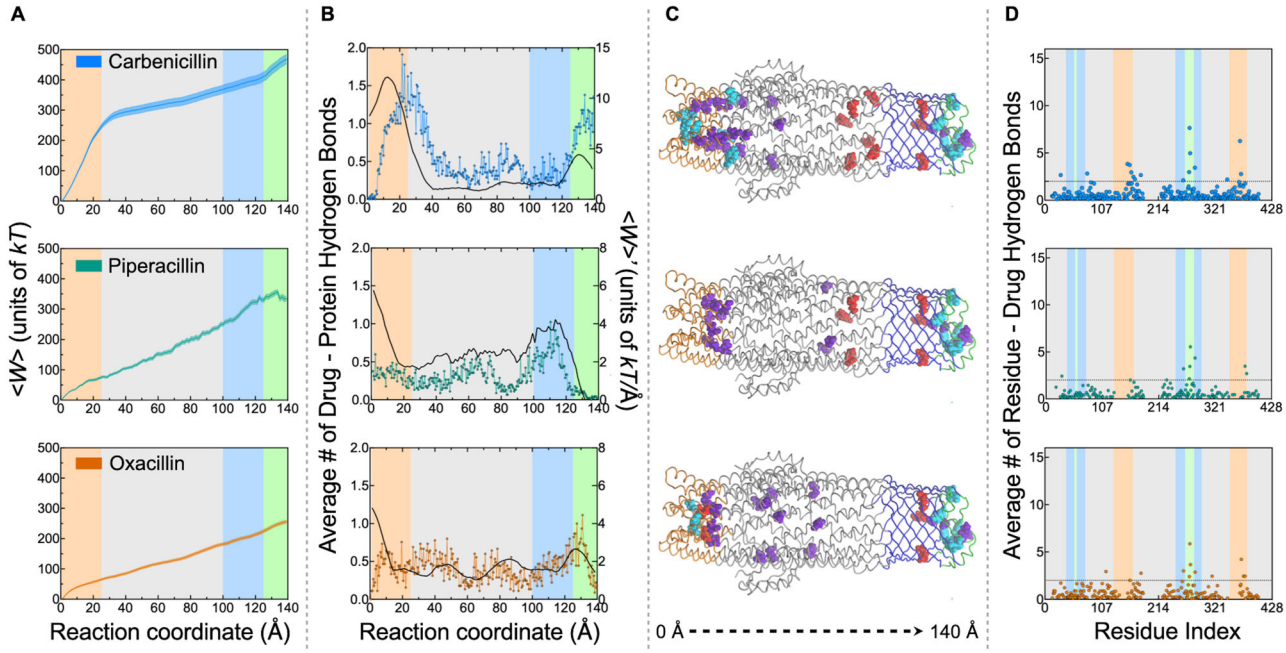

Fig. 5 | Mapping drug-TolC interactions. Carbenicillin (blue; top row), piperacillin (green; middle row), oxacillin (yellow; bottom row). Vertical stripes use the color code of the regions of TolC depicted in Fig. 1B. **A** The work curves from SMD simulations were calculated by binning the reaction coordinate vs. work data. The data were collected at the intervals of 200 fs. (Figures contain whole replicates presented in the source data[67]. Error bars were calculated by block averaging the data in each bin as well as bootstrapping. Errors indicated by shades were less than 10%). **B** The average number of hydrogen bonds between drug and TolC along the reaction coordinate (colored; left y-axis) and the first derivative of the work (black; right y-axis). **C** Residues that have more than an average of two hydrogen bonds (above dashed line in **D**) plotted on the three-dimensional representation of the protein; charged residues red, polars purple, and hydrophobics cyan. **D** Number of hydrogen bonds formed between a given residue and the drug averaged over 45 SMD simulations (hydrogen bond recording timestep is 100 ps for 30 ns long SMD simulations, $N = 45$ for **A**–**D**).

(Fig. 5B). This shift results from basing the reaction coordinate on the pulling atom (purple in Fig. 1C), in contrast to counting hydrogen bonds from any part of the drug molecule and TolC.

Residues that formed two or more hydrogen bonds with selected antibiotics were mainly clustered at the periplasmic tip of the protein (Fig. 5C). For carbenicillin, the polar residues lining the pore played an important role in retarding the progress of the drug movement. Moreover, the hydrophobics at the entry region seemed to form a barrier for carbenicillin and piperacillin but not for oxacillin. The lack of this initial barrier might be the main reason behind the efficient efflux of oxacillin and why it is a nonviable drug for treating Gram-negative infections (Fig. 2 **and** Supplementary Fig. 1). Once the antibiotic molecules overcame the resistance at the TolC entrance region marked by the orange regions in Fig. 5, they accessed the membrane bound part of the pore with relative ease.

We next looked more carefully at the movement of carbenicillin through the protein channel since it experiences a larger number of interactions at the entry to the protein than the other antibiotics and forms extra hydrogen bonds with charged residues in the extracellular barrel region (suggested by the middle peak in Fig. 5B). Supplementary Video 7 illustrates a standard path of carbenicillin. While carbenicillin was moving through the first ~30 Å long region, the triplet salt bridges between R367 and D153 were typically broken. Interestingly, a permanent salt interaction with D371 is established instead (Supplementary Fig. 2A). Here, the negatively charged carbenicillin competed with D153/D371 on the H2/H7 helices. Once carbenicillin moved beyond this region, the drug molecule moved predominantly unhindered through the next 90 Å. In fact, the charged and polar residues aided this last part of the journey by making a hand-over-hand type of coordinated motion that advanced the drug to the outer region of the channel. Finally, in the last ~25 Å, the drug overcame the hydrophobic network of interactions that seal the exit before it finally left the channel. The latter motion is common to all drugs, as exemplified in Supplementary Videos 8 and 9.

Deep mutational scanning of TolC indicates mutations that confer antibiotic sensitivity disrupt the dynamical interaction network and hinder efflux

Using a sequencing-based selection assay, we quantified the fitness impact of single amino acid substitutions across TolC, with carbenicillin, piperacillin, and oxacillin as selection agents. Most positions in TolC showed optimized efflux activity, with few exhibiting notable fitness deviations (Fig. 6A; Supplementary Figs. 3–5). Fifty-one amino acid level replacements in the 428 residues were recorded. Eight mutations were common under all selection conditions; all were sensitivity conferring (Fig. 6A, B). Consistent with the observation that the structure of TolC is less optimized for carbenicillin efflux than for efflux of the other antibiotics, increasing carbenicillin selection strength from 10 μg/ml to 20 μg/ml resulted in a decrease in the number of resistance-conferring mutations and a simultaneous increase in the number of sensitivity-conferring mutations at the periplasmic region of the protein. Nevertheless, the fitness effects of mutations under different carbenicillin concentrations for selection were highly correlated; of the 27 and 32 mutations recorded in the respective concentrations, 23 were common (Fig. 6A, Supplementary Fig. 5).

The mutations common to all selection conditions were clustered in two regions of the protein: S350A/G, A351C, D356G, D371G, and A375T are all near the periplasmic entry region, while the hydrophobic to polar changes V169T and L175G/T occur near the equatorial domain slightly up the channel (the remaining E29P mutation might destabilize protein folding). Sensitivity-conferring mutations clustered at the periplasmic entrance can disrupt the interactions between the adaptor protein and TolC and prevent the operation of the efflux machinery. Another potential function of these mutations is to enhance the interactions with applied antibiotics and, hence, impede the efflux of antibiotics into the extracellular space (Fig. 6B, bottom). When we looked at the specifics of how the mutations depended on the selection agents, we found that evolution again exploits the network of local interactions utilized in efflux. Oxacillin, which has low efficacy

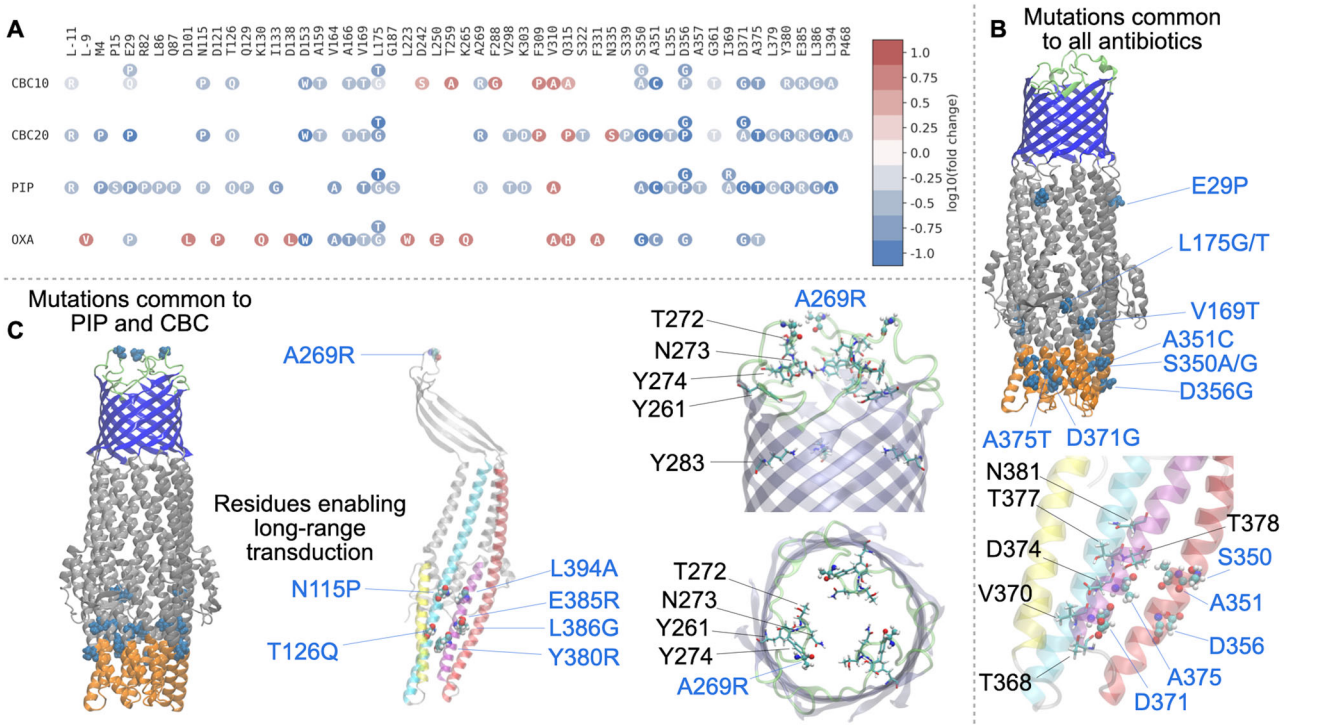

Fig. 6 | Single mutant library selections reveal the TolC residues critical for efflux activity. On all structures, sensitivity conferring residues are labeled in blue and those with a high number of antibiotic interactions in SMD simulations in black (Fig. 5D). **A** Abacus plots summarizing TolC replacements that lead to significant changes in fitness values under selection of carbenicillin (10 μg/ml; CBC10), carbenicillin (20 μg/ml; CBC20), piperacillin (20 μg/ml; PIP), and oxacillin (460 μg/ml; OXA). We used two carbenicillin concentrations to optimize the dynamic range of the fitness values. Excluding synonymous mutations affecting sensitivity, fitness values are represented by a color spectrum from dark blue (more susceptible) to dark red (more resistant). Significance threshold for fitness measurements is 2.5σ (99.4% confidence interval). **B** Sensitivity conferring residues common to all library selections are shown in space filling. The periplasmic entry region of the single protomer shown below (helices colored as in Fig. 3C) displays how sensitivity conferring mutations (CPK representation) are in close proximity to residues that display high interactions with the passing drug (licorice representation). **C** Mutations shared by carbenicillin, and piperacillin are illustrated in space filling on the whole protein structure (left) and on a protomer in the center. The cluster of residues near the equatorial region enable long-range transduction along the major helices and their disruption via mutations alters the upward motions conferring sensitivity to drugs. On the right, extracellular exit site residues are depicted in both side and top views. The exit is controlled by a set of polar residues with high antibiotic interaction counts (licorice); disruption of the hydrophobic gate by the A269R mutation (CPK) residing on the hydrophobic extracellular loop (green) might disrupt the controlled release of the drugs.

against *E. coli* because it is highly effluxable by the AcrAB-TolC, leads to the selection of the least number of deviations and potentially the development of further resistance (Fig. 6A). Conversely, the efflux pump had fewer positions that are prone to developing resistance to carbenicillin and piperacillin; most mutations appearing in these backgrounds led to elevated susceptibility to these drugs. In fact, these drugs have seven additional common mutations (Fig. 6C): those mutations near the equatorial region (N115P and L394A) and those in the region right below (T126Q, Y380R, E385R, L386G) are all in positions where the TolC-carbenicillin/piperacillin interactions are lowest (Fig. 6A and C) and are in the rigid domains (low RMSFs; Fig. 3B). We conjecture that these residues occupy important positions that act as the transducers of the intrinsic efflux motions of TolC reflected in the most dominant PCAs (Supplementary Videos 1–3). Any mutation that 'softens' this rigidity is expected to alter the efflux mechanism and lead to sensitivity. Common mutations in carbenicillin and piperacillin located at the near equatorial and its right below.

At the final exit region, extensive interactions between the drugs and polar/charges residues Y261, T272, N273, Y274, and Y283 are critical to present the drug to the opening of the portal made up of the flexible hydrophobic patch of residues forming the loop, i.e., G268, A269, A270, G271 (Fig. 6C, right). The hydrophobic to polar mutation A269R, which confers sensitivity to both carbenicillin and piperacillin, disrupts the hydrophobic balance near the exit region. This may result from redistributing the network of drug-TolC interactions that contribute to the increased amount of work required to expel the charged drug out of this region. We note that this change would be an entropy dominated shift that involves number and distribution of water molecules near the exit site.

The D371G mutation reveals an allosteric control mechanism spanning the entire efflux pump

Since TolC is optimized for efflux, we tested whether and how these mutations might lead to allosteric effects along with the disrupted local interactions. We selected the D371G mutation that commonly emerged as a sensitivity-conferring mutation in all four of our saturation mutagenesis library selection assays (Fig. 6A). This is counterintuitive since the replacement of aspartate with glycine, a smaller amino acid with no charge, might be expected to increase the volume available to these negatively charged drugs and make it easier for them to be carried away from the initial entry region. D371 is also the top residue providing the highest correlation coefficient in manipulating both the closed-to-open and open-to-closed conformational change in our PRS analysis (Fig. 4C).

We conducted 45 SMD simulations on the D371G mutant with carbenicillin and found the energy required for efflux did not change compared to the wildtype TolC. However, we noted both a minor translation in the curve in the entry region (Fig. 7A–C) and a substantial reduction in hydrogen bonding partners there (Fig. 7C). Drug-free MD simulations showed that the substitution D371G eliminates likely dynamic salt bridges with R367 on the neighboring trimeric chain[13,14,16].

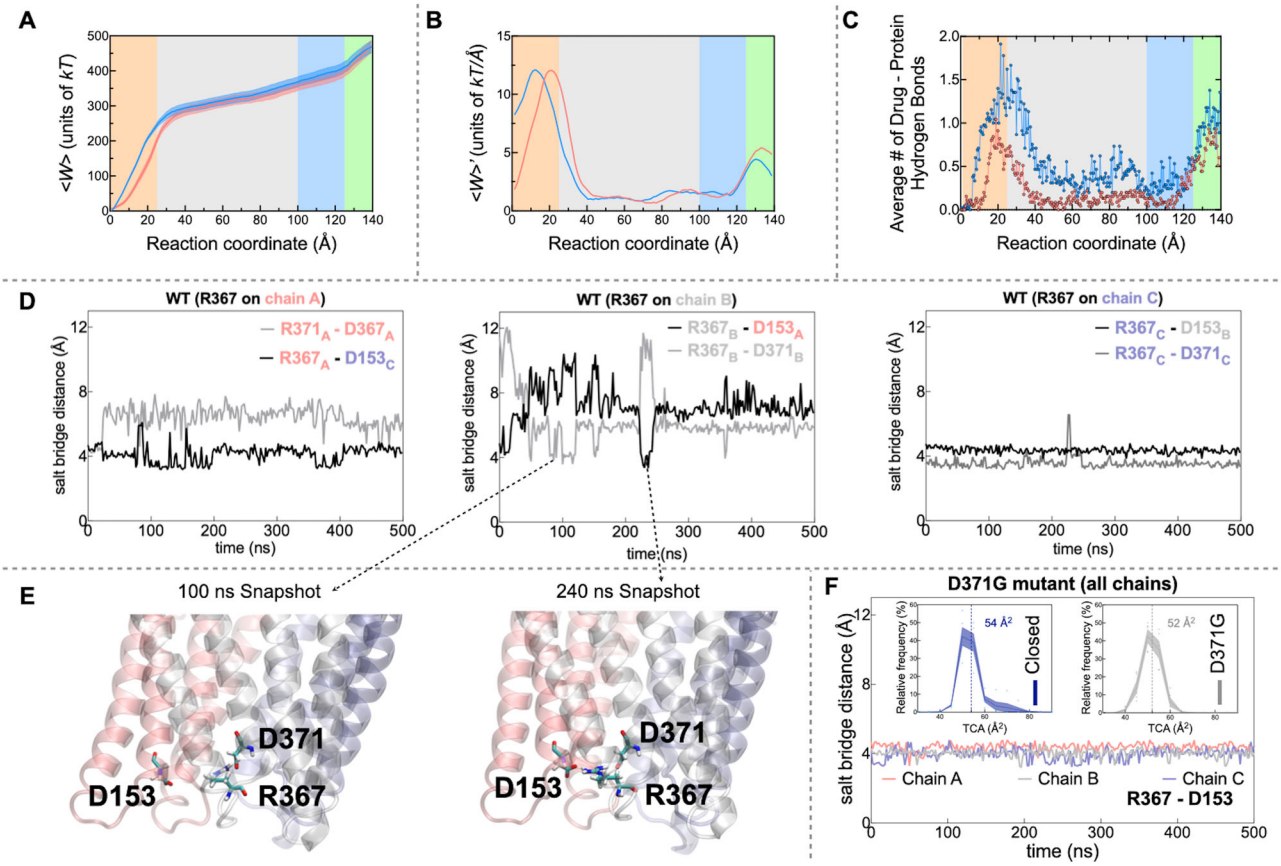

Fig. 7 | The global and local effects of the D371G mutation on TolC. A–C. Carbenicillin SMD findings comparing wild-type and D371G mutant (hydrogen bond recording timestep is 100 ps for 30 ns long SMD simulations, $N = 45$). The average work curves from wild-type closed and D371G structures SMD simulations (Figure contains whole replicates presented in the source data[67]. Error bars were calculated by block averaging the data in each bin as well as bootstrapping. Errors indicated by shades were less than 10%). **B** The first derivative of the average work to understand the interaction sites of the carbenicillin molecule within the protein cavity. We analyzed the required work changes to move carbenicillin through this cavity for closed and D371G mutant protein structures. **D** Dynamical shifts in R367 salt bridges on the three chains of wild-type TolC in the absence of drugs. Manipulation of R367-D153 salt bridge is necessary to provide flexibility for drug entry and initial efflux (see also Supplementary Fig. 2A). R367 has a canonical salt bridge with the D153 on the adjacent chain in the heterotrimer. However, D371 residing on the same chain tends to compete with D153 for this salt bridge. The time evolution of the relevant distances is shown for each chain. **E** Possible R367 side chain positions are shown for time points at 100 ns and 240 ns where the interaction swaps between D371 and D153. **F** These dynamics are completely lost in the mutant; in the MD simulation for the D371G mutant, the D367-D153 interaction remains constant throughout the 500 ns window of observations. The small shrinkage in the TCA with the introduction of the mutation is shown in the inset (see also Supplementary Fig. 2B).

Also, the average TCA of the mutant has a narrower distribution than the wild type of closed form which implies other dynamical interactions are involved in the gating mechanism (Fig. 7F**, inset**). The entry point has a triangular set of interactions that includes the salt bridge between R367 on the loop joining H7/H8 and D153 on H4 (Supplementary Fig. 2). In addition, the nearby D371 on H8 has the potential to form salt bridges with R367 during the dynamical changes that take place in the background fluctuations of the drug free channel as well as during the passage of drugs. The sensitivity conferring mutations at the periplasmic entry observed in all drugs (Fig. 6B) have the effect of disrupting these interactions between the effluxed molecule and TolC. Introducing the mutation D371G removed a negatively charged residue that competed with carbenicillin for the interaction with R367 and resulted in a more permanent salt bridge with D153. Recalling that the TCA fluctuated less in this region (Fig. 3E), we find that this rigidity allowed for a larger volume to accommodate the drug molecule. Paradoxically, this increased the residence time of the drug in the initial trapping region because the dynamical hand-over-hand motions of the drug movement were altered. Moreover, this effect impacted the entire efflux pump (Fig. 7C) and led to the formation of fewer hydrogen bonds along the whole path. We thus conjecture that the D371G mutation caused an allosteric occlusion effect that changed the efflux pattern of the carbenicillin molecule at the extracellular site.

Discussion

TolC is an outer membrane protein involved in several cellular functions, such as efflux of antibiotics, bile salts, dyes and chemicals, entry of colicin and phages, and haemolysin secretion. Its efflux efficiency is highly dependent on the molecules being pumped out. While the overall selectivity of the AcrAB-TolC system for drugs can only be partially explained by what happens to the drug as it passes through TolC, this study focuses on the role of TolC-drug interactions and TolC's contributions to the selectivity once the drug has been delivered to its channel. Here we focus on three β-lactam antibiotics that are effluxed by the TolC at varying rates. The SMD simulations corroborate these findings by quantifying the work done during the efflux and pinpointing interactions that lead to barriers along this path (Fig. 5A). Moreover, the single residues selected by our experimental screen shed further light on the mode of efflux of each drug molecule. For example, movement of piperacillin is mostly retarded in the β-barrel buried in the lipid bilayer near the exit site, while movement of carbenicillin is facilitated both by the hydrophobic plug in the entrance and the hydrophobics lining the first half of the exit pathway (Fig. 5). In fact, our experimental mutational screen (Fig. 6A) revealed that mutations in the first ~40 Å region confer increased sensitivity to TolC through several major mechanisms because decreased efflux of antibiotics results in higher effective concentrations of antibiotic molecules inside the cells (Fig. 6B, C). These mechanisms include

direct interference with dynamical TolC-drug interactions during passage to increase the residence time of the drugs, especially at the entry point. Once an antibiotic enters the channel, the intrinsic movements of TolC assist in transporting the drug through the majority of the channel (Supplementary Videos 7–9). Our experimental results confirm that TolC is highly optimized for oxacillin efflux, a drug that is very similar to methicillin and it replaced its clinical use (Fig. 6A). In fact, any mutations that emerge from our screens are those that further increase resistance of TolC towards this drug. Furthermore, our SMD simulations display the mechanism by which oxacillin is effluxed (Fig. 5, lower panel). Since TolC collective motions are fine tuned for efflux even in the absence of drugs (Figs. 3, 4 and Supplementary Video 3), any free molecule in this space has the tendency to be carried towards the extracellular side. The rigidity maintained by the equatorial region is possibly the facilitator of this efficient efflux mechanism, since we found that key mutations in this region significantly alter the efflux (Fig. 6C). Near the exit, interactions between drug and polar/charged TolC residues form a final barrier before the drug exits the pump. The exit itself is guarded by a hydrophobic patch of residues, which may serve as to gate the entry of pathogens on the extracellular side (Fig. 6C). Altering this region, such as that by the A269R mutation, apparently disrupts the interactions at the exit; the substantially lowered fitness due to this change might be due to an uncontrolled opening of the otherwise well-protected exit that makes the channel leaky in both directions.

Our mutational scanning experiments and MD simulations demonstrate that TolC is an optimally designed molecular machine for efflux. Our findings indicate that evolutionary selection promotes both local interactions and long-range modifications in the system, which in turn augment efflux efficiency and maximize bacterial survival (Fig. 6A). All selected mutations manipulate the network of interactions that work by temporary release of key salt bridges to move the drugs along in a hand-over-hand type of motion (Fig. 7). More importantly, the effects do not stay local and shifts in interactions at one end are conveyed to the other end via intrinsic motions of this pump. This so-called allosteric occlusion effect between entry and exit regions is again a result of the intricate network of interactions. Our work paves the way to use standardized pulling simulations (SMD or similar) to test the effectiveness of newly designed drugs in efflux pumps. Our findings suggest that drugs designed to manipulate interactions in the entry region of TolC have the best chance of circumventing resistance developed during efflux.

We utilized a high-throughput fitness assay to quantify phenotypic changes related to TolC mutations in the presence of β-lactam drugs. As described in detail in the Methods section, we transformed an *E. coli* strain that lacks *tolC* gene with a library of plasmids carrying almost all possible single amino acid replacements in TolC. Although we performed the necessary control experiments in parallel, these assays cannot provide a full mechanistic explanation. For instance, for mutations that sensitize bacterial cells to the β-lactams we tested, there is always a possibility that the mutations hindered efflux activity by causing structural changes that prevent the assembly of the AcrAB-TolC efflux complex. Therefore, we cannot unequivocally rule out such drastic structural changes without conducting additional studies, such as in vitro reassembly of the AcrAB-TolC complex with TolC mutants. These experiments are unfortunately tedious, low-throughput by nature, and beyond our group's current experimental capacity.

In this paper, we focused on mutations that do not target TolC regions that potentially interact with AcrA, based on previous structural studies[29,30]. Instead, in our MD simulations, we studied the effects of mutations that face the inner opening of the TolC trimer. While AcrB is primarily responsible for pumping drug molecules, TolC facilitates efflux as the TolC trimer does not form a passive opening[14]. TolC can open and close in response to structural cues and has many charged residues facing the opening. These residues closely interact with molecules such as antibiotics, bile salts, and toxins. We and others have previously shown that several mutations targeting this region can block antibiotic efflux while still allowing toxin entry, suggesting that the TolC is still intact. Similarly, mutations that block toxin entry but still allow antibiotic efflux have also been reported, which would have been impossible if the TolC function was compromised[31–33].

In our MD simulations, we did not include AcrA and AcrB proteins because of the high computational cost, which is beyond our current resources. Future experimental and computational studies that examine the effects of a select set of TolC mutations in greater detail will likely provide important structural insights. This understanding will help us better comprehend TolC dynamics and guide efforts to develop chemical interventions for maximizing antibiotic efficacy by reducing efflux, thereby increasing the effective antibiotic concentration inside bacterial cells.

Materials and Methods

Molecular dynamics simulations

The closed state x-ray structure (PDBID: 1EK9)[12], and the open state cryo-electron microscopy (cryo-EM) structure (PDBID: 5NG5)[14] were used as the initial TolC coordinates for MD simulations. The D371G mutant which we hypothesized destroyed key salt bridges on the periplasmic entrance side of TolC was also investigated via MD simulations; the initial coordinates of this mutant were created using the Pymol[34]. These coordinates were subjected to MD simulations to understand the time dependent behavior of the protein under physiological conditions. Since TolC is a Gram-negative bacterium protein spanning the outer membrane and the periplasmic space, the orientation of TolC was arranged according to the Orientations of Proteins in Membranes (OPM) database[35,36]. The overall system was prepared on the CHARMM-GUI platform[37–40]. The protein was placed in a bilayer that contains 256 POPE lipids and solvated with TIP3P water molecules. Na^+ and Cl^- ions were added to fulfill the isotonic condition of physiological environment (0.15 M).

MD simulations were performed using NAMD[41,42] and CHARMM36 force field parameters with periodic boundary conditions[38]. The total number of atoms for all our simulations are around 150,000 with box dimensions of $94 \times 94 \times 173$ Å. The particle-mesh Ewald method with a grid spacing of maximal 1 Å per grid in each dimension was used[43]. 12 Å cutoff radius with a switching function turned on at 10 Å was applied to calculate van der Waals (vdW) interactions. The RATTLE algorithm[44] was utilized to set the step size of 2 fs during numerical integration with the Verlet algorithm. Temperature regulation was managed with Langevin using a damping coefficient of 5 ps^{-1}. Pressure regulation was achieved through a Nose-Hoover Langevin piston, and volume variations were set to remain uniform in all directions. Systems were minimized for 50,000 steps to remove undesired van der Waals contacts. The energy-minimized systems were subjected to 5 ns MD run with constant temperature control (*NVT*). The production parts of the MD simulations of length 500 ns were run in the isothermal-isobaric (*NPT*) ensemble at 310 K and 1 atm. The data from MD simulations were analyzed by the open-source Python package ProDy[45–48] as well as custom Python and tcl scripts.

We carried out nine 'free MD simulations' by placing carbenicillin molecule at different locations along the channel. In three of these simulations, carbenicillin molecule located at the periplasmic entry site which corresponds 0–25 Å region of the protein (see Fig. 1B), three are in the central region where the transfer of the drug molecules to the exit region occurs (25-100 Å), and the other three are in the exit region (100–140 Å). We label them entry/transfer/exit and we report results from the averages over 100 ns simulations in each region in Supplementary Fig. S6. The simulation parameters mentioned earlier for closed and open structures were also used for these simulations. The RMSD of C_α atoms for these simulations, and the number of hydrogen bonds in each region during the simulations are shown in the Supplementary Fig. S6. We found that TolC-carbenicillin hydrogen bond densities are the largest in the entry region, very few occur in the transfer region and approximately the one hydrogen bond is maintained by carbenicillin throughout the simulation in the exit region. These occurrences are similar to what we had observed in SMD simulations. Residues display larger than 5% hydrogen bond occupancy at least one of the simulations are displayed in Supplementary Table S2. The only one with

significant overlap which was not observed in our SMD simulations (Fig. 5D) is R143 which is at the periplasmic tip of TolC and is below our docking position for SMD simulations. Therefore, the drugs pulled in SMD simulations are never in contact with this residue.

Principal Component Analysis (PCA)

Our MD simulations cover the sub-μs time scale dynamics of the protein. Normal mode analysis (NMA) models protein as a harmonic oscillating system and determines the protein dynamics around an energetically stable state of the protein. Low-frequency vibrations, also known as low-energy modes, are associated with collective motions, whereas higher-frequency modes are linked to local deformations[49–55]. Principal component analysis (PCA) is an approach for comprehending protein dynamics that involves analyzing an ensemble of conformations obtained from MD simulations[21]. The mathematical principles underlying PCA and NMA share similarities: both require solving linear equations. In PCA, the variance-covariance matrix (**C**) is diagonalized; **C** approximates the inverse of the Hessian matrix employed in NMA[49]. The covariance matrix is constructed using the analysis of multiple snapshots from a MD trajectory, rather than through the calculation of the second derivative near a selected energy minimum. In both instances, the outcomes provide insights into the potential motions a particular structure can undergo, while in a stable conformation. Reducing the dimensions obtained from MD simulations can be advantageous for an unbiased global analysis and to isolate specific configurations. We used principal components to discern the dominant motions of TolC during the MD simulations. PCA was carried out using ProDy[45–48] and the C_α atoms were subjected to analysis. In our previous work we have shown that 40 ns chunks of equilibrated trajectories can sufficiently sample the elastic motions around a selected energy minimum of a protein[56,57]. We have therefore utilized 240–280 and 460–500 ns fragments of the MD trajectories. Extracellular loops and a part of the equatorial domain which displays large motions obscuring the motions of the overall TolC were excluded in the construction of the **C** matrix.

Perturbation Response Scanning (PRS)

The PRS method is a powerful tool we previously developed to identify key residues that are functional in the interconversion of one conformer of a protein into another. PRS uses linear response theory to shed light on the possible conformational changes of protein might undergo by applying external forces on residues in silico[23]. In previous studies[58,59], we and others used PRS to study water-soluble proteins. However, TolC is a transmembrane protein with much larger size and requires embedding the TolC homotrimer in a lipid bilayer. Studying TolC dynamics via PRS also provided us the opportunity to evaluate the utility of this powerful method on membrane proteins and solve possible problems arising from this relatively complex environment.

PRS requires experimentally obtained initial and target coordinates of the C_α atoms of a protein, $\mathbf{S}_{initial}$ and $\mathbf{S}_{target}$, respectively. In our case, these structures were the closed and open forms of TolC. $\mathbf{R_0}$ represents the unperturbed state coordinates (initial), $\mathbf{R_1}$ represents the perturbed state coordinates (target) of the C_α atoms. The external forces vector ($\Delta\mathbf{F}$) in random directions are sequentially applied on each residue of the initial structure. Each predicts displacements in the initial structure, $\Delta\mathbf{R_1}$ by

$$\Delta\mathbf{R}_1 = \langle\mathbf{R}_1\rangle - \langle\mathbf{R}_0\rangle \approx \frac{1}{k_B T}\mathbf{C}\Delta\mathbf{F} \quad (1)$$

where k_B is the Boltzmann constant, and T is temperature in Kelvin units.

A total of 250 random forces are applied to each C_α atom in the protein and results in 250 N predicted displacement vectors, where N is the number of residues. The agreement between experimentally observed and predicted displacements of each residue i in response to the applied force is calculated by Pearson correlation coefficient (C_i) between predicted and experimental displacements. Thus, each $\Delta\mathbf{R_1}$ for applied random forces is compared with the experimentally determined difference between $\mathbf{S}_{initial}$ and $\mathbf{S}_{target}$ coordinates ($\Delta\mathbf{S}$), averaged over all affected residues k:

$$C_i = \sum_{k=1}^{N} \frac{\left[(\Delta R_k)^i - \overline{(\Delta R)^i}\right](\Delta S_k - \overline{\Delta S})}{(N-1)\sigma_R\sigma_S} \quad (2)$$

$\Delta\mathbf{S}_k$ is the experimental displacement between initial MD frame and the target conformation where $\overline{\Delta S}$ the overbar represents average displacement, and σ_R and σ_S denote the standard deviations of experimental and predicted structures, respectively. In this equation, the magnitudes of the displacements, ΔR_k, are compared with ΔS_k. C_i takes on values in the range [0,1] where a correlation greater than 0.7 refers to strong correlation with the experimentally determined conformational changes. PRS was calculated from 240-280 and 460-500 ns chunks of these 500 ns simulations. Extracellular loops and a part of the equatorial domain were excluded in PRS calculations. Since TolC is a homotrimeric outer membrane protein, we performed PRS analysis using each chain as a replica. In the end, obtained results were averaged over 6 sets of data.

Steered Molecular Dynamics (SMD)

We performed SMD calculations using the closed-form TolC structure (PDB ID: 1EK9) as the initial point[12] in separate SMD runs, carbenicillin, piperacillin, or oxacillin was positioned at the periplasmic tip of the protein by docking, CB-Dock2 tool[60]. The charges of carbenicillin, piperacillin, and oxacillin in water are −2, −1, and −1, respectively. While these charges might shift depending on the position of the drugs in the protein environment, we assumed the pKa of all positions and the charges remained constant in our simulations. The simulation boxes for the membrane, protein, and three different antibiotic molecules were optimized using the CHARMM-GUI web server as described in the "MD simulations" section. Force fields for the antibiotic molecules used in our study were generated by CHARMM general force field module of CHARMM-GUI[39,61,62]. The systems obtained with the three different antibiotics were minimized for 50,000 steps and equilibrated for 0.5 ns. A 50 kcal mol^{-1} $Å^{-2}$ harmonic spring constant was applied to a carbon atom on the hexane structure of antibiotic molecules (depicted as purple spheres in Fig. 1C) for forcing the drug molecule pass through the TolC channel, a value that satisfies the stiff spring approximation[63]. Antibiotics were pulled along the z-axis until they reached the extracellular loops of the protein at a constant velocity of 5 Å ns^{-1}. The molecules traveled approximately 140 Å; each SMD simulation thus lasts nearly 30 ns. No restraints were applied to the substrates in the x and y directions. The pulling simulations of each antibiotic molecule were repeated 45 times to increase the signal-to-noise ratio. The average work done to reach the extracellular side was then calculated for each antibiotic molecule. We note that the general trends and the energy levels in the work curves did not change when the pulling atom was modified to the nitrogen atom in the middle of the carbenicillin molecule from the carbon atom on the hexane ring. Also, modification of the pulling velocity to 0.5 Å ns^{-1} from 5 Å ns^{-1} did not change the profiles in the first 30 Å of the pump. We found that residues that are in contact with the carbenicillin above the threshold we have set in Fig. 5D overlap with our 0.5 Å ns^{-1} pulling simulations. We thus concluded that doing 45 pulling simulations at 5 Å ns^{-1} provides the information necessary to compare our simulation findings with our mutational scanning experiments.

Bacterial Strains and Growth Conditions. *Escherichia coli* (*E. coli*) cells were grown at 37 °C in a M9 minimal medium supplemented with 0.4% glucose and 0.2% amicase. The BW25113 *E. coli* strain (CGSC No.: 7636) and the *ΔtolC732::kan E. coli* strain (CGSC No.: 11430) were obtained from Coli Genetic Stock Center[31]. Using the method from reference[64], we removed the kanamycin resistance marker in the *ΔtolC732::kan E. coli* strain. In the article, we refer to the *E. coli* strain *tolC* gene deletion as *ΔtolC* strain.

The *tolC* gene from BW25113 (wild type, WT) strain was PCR amplified using 5′-ATTCAAAGGAGGTACCCACCATGAAGAAAT

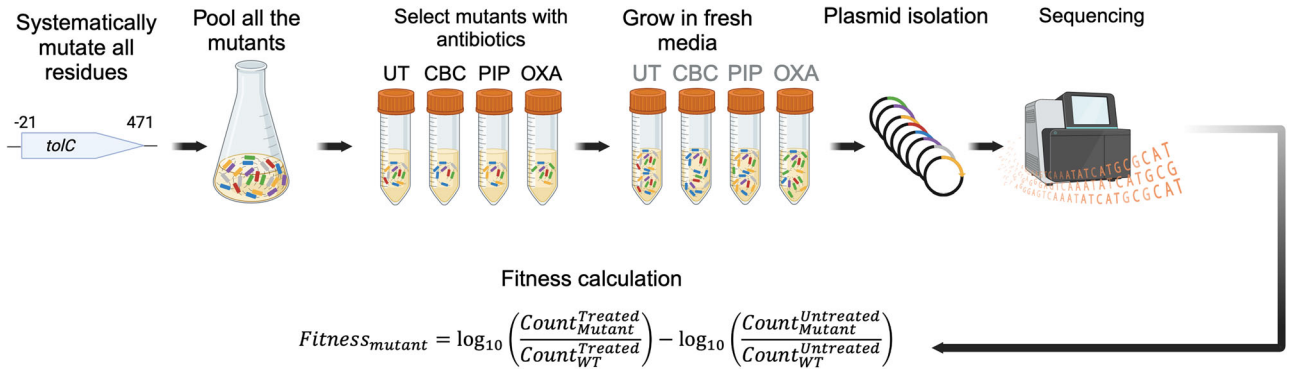

Fig. 8 | Selection assay protocol. We conducted deep mutational scanning on TolC, systematically mutating all 493 residues, which includes the 21-amino acid long signal sequence preceding the start codon (excluding it). Residues were mutated to all the 19 other amino acids, along with the stop codon. Obtained mutants were pooled together and grown overnight. Overnight grown mutant pool and *ΔtolC* strains were split into cultures: untreated (UT), CBC, PIP, OXA; the experiment was replicated once. Cultures other than the untreated were treated with the relevant selection factors. Cultures were exposed to drugs for 3 h for selection. This was followed by 6 hours long incubation in fresh growth media without any selection agent for the recovery of cells (gray abbreviations on the tubes represent previously applied antibiotics). We isolated *tolC* mutant carrying plasmids and PCR amplified the *tolC* gene for amplicon sequencing. Mutation frequencies were calculated by deep sequencing and fitness values of each mutation were calculated using the formula in the figure. (Created with BioRender.com).

TGCTCCCCATTC-3′ (forward), and 5′-AGAAATCGATTGTATCA GTCTCAGTTACGGAAAGGGTTATGAC-3′ (reverse) primers. PCR amplified *tolc* gene was then cloned into the pSF-Oxb14 plasmid which was obtained from Oxford Genetics (OGS557, Sigma) using the NEBuilder HiFi DNA Assembly kit (New England Biolabs); by strictly following the protocols recommended by the manufacturers. The resulting plasmid (pSF-Oxb14-*tolC*) contains kanamycin resistance cassette and an Oxb14 constitutively open promoter region. The introduced *E. coli tolc* gene sequence was confirmed by Sanger sequencing.

Whole gene saturation mutagenesis library (SML) for each codon in the *tolC* gene used in our experiments was carried out by two separate PCR reactions for each codon in the *tolC* gene. First, a portion of *tolC* gene in the pSF-Oxb14-*tolC* plasmid was amplified and the target codon was randomized using a primer containing NNS nucleotide sequence (where N represents A, C, G, or T, and S represents G or C nucleotides). The first PCR products were referred as insert. Second PCR reaction amplifies the remainder of pSF-Oxb14-*tolC* plasmid which is referred as backbone. The custom software to design mutagenesis primers is available (See https://github.com/ytalhatamer/DMS_PrimerDesignTool). The PCR products (insert and backbone) were assembled using NEBuilder HiFi DNA Assembly Kit (E5520, New England Biolabs), and the resulting plasmids were introduced into NEB-5-alpha cells (C2987, New England Biolabs). Plasmids were extracted from the transformed cells using the Nucleospin Plasmid kit. This assay resulted in libraries for each residue. Equimolar amounts of the library were pooled into 5 sublibraries and these pooled sublibraries were transformed into *ΔtolC* strain for selection experiments[31]. We refer to this library as TolC-SML. We refer the *ΔtolC* strain supplemented with *the* pSF-Oxb14-t*olC plasmid as ΔtolC*+p*tolC*. All selection experiments were conducted with minimal M9 media containing 50 μg ml^{-1} of kanamycin to prevent loss of the pSF-Oxb14-t*olC* plasmid.

Determination of minimum inhibitory concentrations (MIC)

Bacterial cells were overnight grown and optical densities (OD600) of cultures were measured in a 1 cm pathlength cuvette. OD600 was then adjusted to 0.001 for which corresponds ~5×10^5 colony forming unit (CFU) per milliliters. Bacterial cells were then grown in 96 well plates (~ 200 μl per well) in which drug gradients were created using serial dilutions (Fig. 2A). Highest starting antibiotic concentrations on these plates were 100 μg/ml for carbenicillin, 20 μg/ml for piperacillin, and 1875 μg/ml for oxacillin. The dilution factor for carbenicillin and piperacillin was 1/2 while it was 1/5 for oxacillin. These 96-wells were incubated for 18 hours in a humidity-controlled shaker operated at 37 °C and 400 RPM. After the overnight incubation, cell densities were measured using a plate reader (VictorX, PerkinElmer). The experiments were performed in triplicates for each antibiotic molecule. For each strain and antibiotic compounds, the MIC value was defined as the lowest antibiotic concentration at which the final OD600 was below ~0.04 after background correction.

Selection Assay

We used three antibiotics: carbenicillin, piperacillin, and oxacillin as selection agents. We used the saturation mutagenesis library (SML) for *tolC*[31]. In this library, all residues except start codon (471 residues in the mature TolC protein, and the 22 residue-long signal sequence) were mutated to all other possible residues, and a pool of mutant library was generated (Fig. 8). We measured the fitness effects of mutations under selection using a liquid-based sequencing assay. Our assay does not allow us to evaluate the expression levels or stability of thousands of TolC mutants. However, by completing the screen with three different antibiotics, we can confidently deduce that a TolC mutant is expressed and stable enough if the relative fitness of the mutant under the selection with at least one antibiotic, with respect to the wild-type TolC, is non-deleterious, suggesting that the efflux for at least one antibiotic is still occurring.

We grew *the* mutant library in M9 minimal medium supplemented with 0.4% glucose and 0.2% amicase overnight, diluted to a final optical density of 0.001, and then exposed these cultures to one of the selection factors: carbenicillin, piperacillin, and oxacillin for 3 h at 37 °C, 400 rotation per minute (RPM). In parallel, we grew cultures without any selection (untreated: UT) for separating drug-induced fitness effects from other potential fitness effects that are not related with the bactericidal effects of antibiotics. The concentrations for these antibiotics in this selection assay were 20 μg/ml and 10 μg/ml for carbenicillin, 10 μg/ml for piperacillin, and 460 μg/ml for oxacillin. These concentrations were close to the MIC of the related compound (Fig. 2B–D). We note that for carbenicillin we used two carbenicillin concentrations because the dynamic range of the fitness values was not large enough when the selection was done with the lower concentration. The dose-response curve for carbenicillin is very steep (higher Hill coefficient), making it difficult to adjust the selection strength.

At the end of the selection period, these cultures were spun down at 5000 × g for 5 minutes. The pellets obtained from spinning were resuspended in fresh M9 minimal medium supplemented with 0.4% glucose, 0.2% amicase and 50 μg/ml kanamycin and incubated at 37°C, 400 RPM for 6 hours to increase cell density and ensure harvesting of enough *tolC* carrying plasmid for sequencing. We recorded cell densities during this recovery period as depicted in Supplementary Fig. 1. Cells were harvested by

spinning cultures at 5000 × g for 5 minutes. Pellets were collected for plasmid purification. *tolC* gene variants on these plasmids were amplified with polymerase chain reaction (PCR) using 5'-TACCCGGCAGATCTTTGTCGATCCTA-3' (forward), and 5'-GTGAGCTGAAGGTACGCTGTATCTCA-3' (reverse) primers.

These products were sequenced on Illumina NovaSeq 6000, producing 151 bp reads. Sequence reads were compared with the wild type *tolC* sequence and mutations were listed. Sequence reads that had mutations in more than one residue were excluded from the analysis. Synonymous mutations yielding the same amino acid replacement were grouped together and used as a reference for relative fitness calculations. The frequency of each mutation was calculated by dividing the number of counts for that mutation with the number of all reads, including alleles with multiple mutations[31]. We then used the formula displayed in Fig. 8 to calculate relative fitness effects of each mutation.

Statistics and Reproducibility. MD simulations were performed for 500 ns. The average RMSF graph was plotted for the homotrimeric TolC protein. The data points for chain RMSFs were plotted as pale dots. The principal components (PC) and perturbation response scanning (PRS) analyses were performed on two chunks from the related trajectory. The *p-value* for PRS data were calculated by one-sample two-tailed t-test, results were reproducible ($p < 0.01$). SMD simulations have 45 replicates for each antibiotic molecule, antibiotic-work curves for each run are available. Work data were collected for each 200 fs. Error bars for work graphs were determined by using block averaging for the data in each bin, and by applying the bootstrapping method (See Fig. 5A and Fig. 7A). Significance threshold for fitness measurements is 2.5σ (99.4% confidence interval).

Reporting summary

Further information on research design is available in the Nature Portfolio Reporting Summary linked to this article.

Data availability

Figures, supplementary materials and source data to generate presented figures were deposited online[65–69]. Graphs were prepared using the Graphpad Prism software. The custom software to design mutagenesis primers is available at https://github.com/ytalhatamer/DMS_PrimerDesignTool.

Code availability

NAMD 2.13 & 2.14, and ProDy were used to run and analyze performed simulations. Raw amplicon sequencing data for the mutagenesis experiment are deposited under the NCBI BioProject with accession number PRJNA1078904 and available at following URL: https://www.ncbi.nlm.nih.gov/bioproject/PRJNA1078904. Original code generated for producing the results for this study is deposited at GitHub at the following repository: https://github.com/midstlab/Kantarcioglu_2024[69]. Any additional data provided in this paper will be provided by the lead contact upon request.

Received: 12 March 2024; Accepted: 16 August 2024;
Published online: 26 August 2024

References

1. Paulsen, I. T., Park, J. H., Choi, P. S. & Saier, M. H. A family of Gram-negative bacterial outer membrane factors that function in the export of proteins, carbohydrates, drugs and heavy metals from Gram-negative bacteria. *FEMS Microbiol. Lett.* **156**, 1–8 (2006).
2. Nikaido, H. Multidrug efflux pumps of gram-negative bacteria. *J. Bacteriol.* **178**, 5853–5859 (1996).
3. Nikaido, H. Multidrug Resistance in Bacteria. *Annu. Rev. Biochem.* **78**, 119–146 (2009).
4. Levy, S. B. & Marshall, B. Antibacterial resistance worldwide: causes, challenges and responses. *Nat. Med.* **10**, S122–S129 (2004).
5. Poole, K. Outer Membranes and Efflux: The Path to Multidrug Resistance in Gram- Negative Bacteria. *Curr. Pharm. Biotechnol.* **3**, 77–98 (2002).
6. Nikaido, H. Structure and Mechanism of RND-Type Multidrug Efflux Pumps. In *Advances in Enzymology - and Related Areas of Molecular Biology* (ed. Toone, E. J.) vol. 77 1–60 (Wiley, 2011).
7. Fralick, J. A. Evidence that TolC is required for functioning of the Mar/AcrAB efflux pump of Escherichia coli. *J. Bacteriol.* **178**, 5803–5805 (1996).
8. Piddock, L. J. V. Multidrug-resistance efflux pumps? not just for resistance. *Nat. Rev. Microbiol.* **4**, 629–636 (2006).
9. Darzynkiewicz, Z. M. et al. Identification of Binding Sites for Efflux Pump Inhibitors of the AcrAB-TolC Component AcrA. *Biophys. J.* **116**, 648–658 (2019).
10. Ayhan, D. H. et al. Sequence-Specific Targeting of Bacterial Resistance Genes Increases Antibiotic Efficacy. *PLOS Biol.* **14**, e1002552 (2016).
11. Puchta, O. et al. Network of epistatic interactions within a yeast snoRNA. *Science* **352**, 840–844 (2016).
12. Koronakis, V., Sharff, A., Koronakis, E., Luisi, B. & Hughes, C. Crystal structure of the bacterial membrane protein TolC central to multidrug efflux and protein export. *Nature* **405**, 914–919 (2000).
13. Bavro, V. N. et al. Assembly and Channel Opening in a Bacterial Drug Efflux Machine. *Mol. Cell* **30**, 114–121 (2008).
14. Wang, Z. et al. An allosteric transport mechanism for the AcrAB-TolC multidrug efflux pump. *eLife* **6**, e24905 (2017).
15. Pei, X.-Y. et al. Structures of sequential open states in a symmetrical opening transition of the TolC exit duct. *Proc. Natl Acad. Sci.* **108**, 2112–2117 (2011).
16. Marshall, R. L. & Bavro, V. N. Mutations in the TolC Periplasmic Domain Affect Substrate Specificity of the AcrAB-TolC Pump. *Front. Mol. Biosci.* **7**, 166 (2020).
17. Atilgan, A. R. et al. Anisotropy of Fluctuation Dynamics of Proteins with an Elastic Network Model. *Biophys. J.* **80**, 505–515 (2001).
18. Phan, G. et al. Structural and Dynamical Insights into the Opening Mechanism of P. aeruginosa OprM Channel. *Structure* **18**, 507–517 (2010).
19. Newman, K. E. & Khalid, S. Conformational dynamics and putative substrate extrusion pathways of the N-glycosylated outer membrane factor CmeC from Campylobacter jejuni. *PLOS Comput. Biol.* **19**, e1010841 (2023).
20. Izrailev, S., Stepaniants, S., Balsera, M., Oono, Y. & Schulten, K. Molecular dynamics study of unbinding of the avidin-biotin complex. *Biophys. J.* **72**, 1568–1581 (1997).
21. Jolliffe, I. Principal Component Analysis. in *Encyclopedia of Statistics in Behavioral Science* (eds. Everitt, B.S. & Howell, D.C.) https://doi.org/10.1002/0470013192.bsa501 (Wiley, 2005).
22. Lange, O. F. et al. Recognition Dynamics Up to Microseconds Revealed from an RDC-Derived Ubiquitin Ensemble in Solution. *Science* **320**, 1471–1475 (2008).
23. Atilgan, C. & Atilgan, A. R. Perturbation-Response Scanning Reveals Ligand Entry-Exit Mechanisms of Ferric Binding Protein. *PLoS Comput. Biol.* **5**, e1000544 (2009).
24. Atilgan, C., Gerek, Z. N., Ozkan, S. B. & Atilgan, A. R. Manipulation of Conformational Change in Proteins by Single-Residue Perturbations. *Biophys. J.* **99**, 933–943 (2010).
25. Penkler, D. L., Atilgan, C. & Tastan Bishop, Ö. Allosteric Modulation of Human Hsp90α Conformational Dynamics. *J. Chem. Inf. Model.* **58**, 383–404 (2018).
26. Ross, C. J., Atilgan, A. R., Tastan Bishop, Ö. & Atilgan, C. Unraveling the Motions behind Enterovirus 71 Uncoating. *Biophys. J.* **114**, 822–838 (2018).
27. Weng, J. & Wang, W. Structural Features and Energetics of the Periplasmic Entrance Opening of the Outer Membrane Channel TolC

Revealed by Molecular Dynamics Simulation and Markov State Model Analysis. *J. Chem. Inf. Model.* **59**, 2359–2366 (2019).
28. Vaccaro, L., Scott, K. A. & Sansom, M. S. P. Gating at Both Ends and Breathing in the Middle: Conformational Dynamics of TolC. *Biophys. J.* **95**, 5681–5691 (2008).
29. Weeks, J. W., Celaya-Kolb, T., Pecora, S. & Misra, R. AcrA suppressor alterations reverse the drug hypersensitivity phenotype of a TolC mutant by inducing TolC aperture opening. *Mol. Microbiol.* **75**, 1468–1483 (2010).
30. Gerken, H. & Misra, R. Genetic evidence for functional interactions between TolC and AcrA proteins of a major antibiotic efflux pump of *Escherichia coli*. *Mol. Microbiol.* **54**, 620–631 (2004).
31. Tamer, Y. T. et al. The Antibiotic Efflux Protein TolC Is a Highly Evolvable Target under Colicin E1 or TLS Phage Selection. *Mol. Biol. Evol.* **38**, 4493–4504 (2021).
32. German, G. J. & Misra, R. The TolC protein of Escherichia coli serves as a cell-surface receptor for the newly characterized TLS bacteriophage. *J. Mol. Biol.* **308**, 579–585 (2001).
33. Masi, M., Vuong, P., Humbard, M., Malone, K. & Misra, R. Initial Steps of Colicin E1 Import across the Outer Membrane of *Escherichia coli*. *J. Bacteriol.* **189**, 2667–2676 (2007).
34. Schrödinger, LLC. The PyMOL Molecular Graphics System, Version 1.8. (2015).
35. Lomize, M. A., Pogozheva, I. D., Joo, H., Mosberg, H. I. & Lomize, A. L. OPM database and PPM web server: resources for positioning of proteins in membranes. *Nucleic Acids Res* **40**, D370–D376 (2012).
36. Lomize, A. L., Todd, S. C. & Pogozheva, I. D. Spatial arrangement of proteins in planar and curved membranes by PPM 3.0. *Protein Sci.* **31**, 209–220 (2022).
37. Jo, S., Kim, T. & Im, W. Automated Builder and Database of Protein/Membrane Complexes for Molecular Dynamics Simulations. *PLoS ONE* **2**, e880 (2007).
38. Lee, J. et al. CHARMM-GUI Input Generator for NAMD, GROMACS, AMBER, OpenMM, and CHARMM/OpenMM Simulations Using the CHARMM36 Additive Force Field. *J. Chem. Theory Comput.* **12**, 405–413 (2016).
39. Jo, S., Kim, T., Iyer, V. G. & Im, W. CHARMM-GUI: A web-based graphical user interface for CHARMM. *J. Comput. Chem.* **29**, 1859–1865 (2008).
40. Best, R. B. et al. Optimization of the Additive CHARMM All-Atom Protein Force Field Targeting Improved Sampling of the Backbone ϕ, ψ and Side-Chain χ_1 and χ_2 Dihedral Angles. *J. Chem. Theory Comput.* **8**, 3257–3273 (2012).
41. Phillips, J. C. et al. Scalable molecular dynamics with NAMD. *J. Comput. Chem.* **26**, 1781–1802 (2005).
42. Phillips, J. C. et al. Scalable molecular dynamics on CPU and GPU architectures with NAMD. *J. Chem. Phys.* **153**, 044130 (2020).
43. Essmann, U. et al. A smooth particle mesh Ewald method. *J. Chem. Phys.* **103**, 8577–8593 (1995).
44. Andersen, H. C. Rattle: A "velocity" version of the shake algorithm for molecular dynamics calculations. *J. Comput. Phys.* **52**, 24–34 (1983).
45. Bakan, A. & Bahar, I. The intrinsic dynamics of enzymes plays a dominant role in determining the structural changes induced upon inhibitor binding. *Proc. Natl Acad. Sci.* **106**, 14349–14354 (2009).
46. Bakan, A., Meireles, L. M. & Bahar, I. ProDy: Protein Dynamics Inferred from Theory and Experiments. *Bioinformatics* **27**, 1575–1577 (2011).
47. Bakan, A. et al. *Evol* and *ProDy* for bridging protein sequence evolution and structural dynamics. *Bioinformatics* **30**, 2681–2683 (2014).
48. Zhang, S. et al. *ProDy* 2.0: increased scale and scope after 10 years of protein dynamics modelling with Python. *Bioinformatics* **37**, 3657–3659 (2021).
49. Bahar, I., Lezon, T. R., Bakan, A. & Shrivastava, I. H. Normal Mode Analysis of Biomolecular Structures: Functional Mechanisms of Membrane Proteins. *Chem. Rev.* **110**, 1463–1497 (2010).
50. Henzler-Wildman, K. A. et al. Intrinsic motions along an enzymatic reaction trajectory. *Nature* **450**, 838–844 (2007).
51. Henzler-Wildman, K. A. et al. A hierarchy of timescales in protein dynamics is linked to enzyme catalysis. *Nature* **450**, 913–916 (2007).
52. Brooks, B. R., Janežič, D. & Karplus, M. Harmonic analysis of large systems. I. Methodology. *J. Comput. Chem.* **16**, 1522–1542 (1995).
53. Case, D. A. Normal mode analysis of protein dynamics. *Curr. Opin. Struct. Biol.* **4**, 285–290 (1994).
54. Skjaerven, L., Martinez, A. & Reuter, N. Principal component and normal mode analysis of proteins; a quantitative comparison using the GroEL subunit. *Proteins Struct. Funct. Bioinforma.* **79**, 232–243 (2011).
55. Bauer, J. A. & Pavlović, J. & Bauerová-Hlinková, V. Normal Mode Analysis as a Routine Part of a Structural Investigation. *Molecules* **24**, 3293 (2019).
56. Atilgan, C., Okan, O. B. & Atilgan, A. R. Network-Based Models as Tools Hinting at Nonevident Protein Functionality. *Annu. Rev. Biophys.* **41**, 205–225 (2012).
57. Okan, O. B., Atilgan, A. R. & Atilgan, C. Nanosecond Motions in Proteins Impose Bounds on the Timescale Distributions of Local Dynamics. *Biophys. J.* **97**, 2080–2088 (2009).
58. Penkler, D., Sensoy, Ö., Atilgan, C. & Tastan Bishop, Ö. Perturbation–Response Scanning Reveals Key Residues for Allosteric Control in Hsp70. *J. Chem. Inf. Model.* **57**, 1359–1374 (2017).
59. Jalalypour, F., Sensoy, O. & Atilgan, C. Perturb–Scan–Pull: A Novel Method Facilitating Conformational Transitions in Proteins. *J. Chem. Theory Comput.* **16**, 3825–3841 (2020).
60. Liu, Y. et al. CB-Dock2: improved protein–ligand blind docking by integrating cavity detection, docking and homologous template fitting. *Nucleic Acids Res* **50**, W159–W164 (2022).
61. Brooks, B. R. et al. CHARMM: The biomolecular simulation program. *J. Comput. Chem.* **30**, 1545–1614 (2009).
62. Kim, S. et al. CHARMM-GUI ligand reader and modeler for CHARMM force field generation of small molecules: CHARMM-GUI Ligand Reader and Modeler for CHARMM Force Field Generation of Small Molecules. *J. Comput. Chem.* **38**, 1879–1886 (2017).
63. Nategholeslam, M., Gray, C. G. & Tomberli, B. Stiff Spring Approximation Revisited: Inertial Effects in Nonequilibrium Trajectories. *J. Phys. Chem. B* **121**, 391–403 (2017).
64. Datsenko, K. A. & Wanner, B. L. One-step inactivation of chromosomal genes in *Escherichia coli* K-12 using PCR products. *Proc. Natl Acad. Sci.* **97**, 6640–6645 (2000).
65. Kantarcioglu, I. et al. Structural Shifts in TolC Facilitate Efflux-Mediated β-lactam Resistance - Supplementary Videos. figshare. Media. https://doi.org/10.6084/m9.figshare.26347309.v2 (2024).
66. Kantarcioglu, I. et al. Structural Shifts in TolC Facilitate Efflux-Mediated β-lactam Resistance - Supplementary Tables. 25647 Bytes figshare https://doi.org/10.6084/M9.FIGSHARE.26352334.V1 (2024).
67. Kantarcioglu, I. et al. Structural Shifts in TolC Facilitate Efflux-Mediated β-lactam Resistance - Source Data. 3167173 Bytes figshare https://doi.org/10.6084/m9.figshare.26352316.v3 (2024).
68. Kantarcioglu, I. et al. *Structural Shifts in TolC Facilitate Efflux-Mediated β-Lactam Resistance - Figures*. 53935550 Bytes figshare https://doi.org/10.6084/m9.figshare.26352325.v2 (2024).
69. MIDST lab. midstlab/Kantarcioglu_2024: Kantarcioglu_2024. Zenodo https://doi.org/10.5281/ZENODO.12749498 (2024).

Acknowledgements

The numerical calculations reported in this paper were partially performed at TUBITAK ULAKBIM, High Performance and Grid Computing Center (TRUBA resources). We thank TUBITAK project no. 122F149 for partial support. I.K. was partially supported by TUBITAK 2214-A visiting research fellowship (Application Number: 1059B142100453). E.T. is supported by UTSW Endowed Scholars Program, Human Frontiers Science Program Research

grant RGP0042/2013, NIH grant R01GM125748, DOD PR172118, and Welch Foundation I-2082-20210327. We thank Alan Katz for a careful reading of the manuscript.

Author contributions

I.K: Data acquisition, methodology, writing, conceptualization, investigation. I.K.G: Data acquisition, methodology. T.F.G: Methodology. M.S.K: Methodology. A.R.A: Supervision, writing, investigation, methodology. E.T.: Funding acquisition, writing, methodology, project administration, supervision, conceptualization, investigation. C.A.: Funding acquisition, writing, methodology, project administration, supervision, conceptualization, investigation.

Competing interests

The authors declare no competing interests.

Additional information

Supplementary information The online version contains supplementary material available at https://doi.org/10.1038/s42003-024-06750-0.

Correspondence and requests for materials should be addressed to Erdal Toprak or Canan Atilgan.

Peer review information *Communications Biology* thanks the anonymous reviewers for their contribution to the peer review of this work. Primary Handling Editors: Wendy Mok and Laura Rodríguez Pérez. A peer review file is available.